September 4, 2018
DESY 18-155

Strong gravitational radiation from a simple dark matter model

Iason Baldes and Camilo Garcia-Cely

DESY, Notkestraße 85, D-22607 Hamburg, Germany

iason.baldes@desy.de, camilo.garcia.cely@desy.de

Abstract

A rather minimal possibility is that dark matter consists of the gauge bosons of a spontaneously broken symmetry. Here we explore the possibility of detecting the gravitational waves produced by the phase transition associated with such breaking. Concretely, we focus on the scenario based on an $SU(2)_D$ group and argue that it is a case study for the sensitivity of future gravitational wave observatories to phase transitions associated with dark matter. This is because there are few parameters and those fixing the relic density also determine the effective potential establishing the strength of the phase transition. Particularly promising for LISA is the super-cool dark matter regime, with DM masses above 100 TeV, for which we find that the gravitational wave signal is notably strong. In our analysis, we include the effect of astrophysical foregrounds, which are often ignored in the context of phase transitions.

Contents

1 Introduction

Cosmological and astrophysical observations strongly suggest that, in contrast to the ordinary substances found on Earth, baryons are not the dominant constituent of the matter in the Universe [1]. Such non-baryonic matter is called dark because its interactions with the Standard Model (SM) particles — particularly with photons — are constrained to be very weak. This, along with the obvious fact that dark matter (DM) must be stable on cosmological timescales, are the two most important properties of any DM candidate.

The first property is often invoked as an argument for the electroweak nature of DM interactions. In fact, models where DM is directly coupled to the W or Z bosons naturally explain the DM relic density by means of the thermal freeze-out of DM annihilations in the Early Universe. Nevertheless, these scenarios have been dramatically constrained in the past couple of decades by direct and indirect detection experiments, together with colliders, most recently the LHC [2–4]. In contrast, models where DM is directly coupled to the Higgs and not to the W or Z bosons are much less constrained by the aforementioned experiments, especially in regimes where the DM is heavier than the Higgs boson. Interestingly, gravitational waves (GWs) offer a new complementary way to probe the latter scenarios. This is because they typically require the existence of additional scalar fields, which can potentially trigger a first-order phase transition (PT) in the Early Universe and therefore the emission of GWs [5–8]. Of course, DM can be probed in this way only if its properties are closely related to the PT [9–11]. This is the subject of the present work.

In order to motivate a concrete choice for the DM model, we will invoke the second DM property mentioned above, i.e. its stability. This is often ensured by imposing a discrete

symmetry in the DM sector. The most common examples being Z_2 symmetries or the so-called R-parity in supersymmetric theories. Nevertheless, such symmetries are not known to exist in nature.[1] Better-motivated scenarios are those where DM is stable as a result of its own dynamics. In fact, this is exactly what happens with the stable particles of the SM. For instance, proton stability follows from baryon number conservation, which is an accidental symmetry due to the $SU(3)_C \times SU(2)_L \times U(1)_Y$ charges of the matter fields. An incomplete list of examples of this type of scenarios include Minimal DM [12], spin-one DM models [13–16] and QCD-like models of DM [17].

The previous observations motivate us to study the spin-one DM model proposed in [13], in which the DM portal to the SM is the Higgs boson. Concretely, we extend the SM with a dark $SU(2)_D$ local symmetry, under which all the SM particles are assumed to be singlets. In addition, we postulate a dark scalar doublet which carries no SM charges and whose vacuum expectation value (VEV) breaks the $SU(2)_D$ symmetry via a Higgs mechanism in the dark sector, ensuring the theoretical consistency of the model containing massive spin-one fields. After symmetry breaking, the particle content includes — besides the SM — three mass-degenerate particles of spin-one and one dark Higgs boson. An accidental global $SO(3)$ symmetry remains after symmetry breaking which forbids the decay of the gauge bosons. Collectively, these comprise our DM candidate, which only couples to itself, to the SM Higgs h, and to the dark Higgs h_D. The Higgs portal interaction allows h_D to decay to light SM particles, thus avoiding it becoming a DM component.

We will consider two production regimes for the DM relic density. First, the standard thermal freeze-out of DM annihilations into dark Higgs bosons. Second, a more exotic possibility in which we assume a classically scale invariant potential for our model [18]. As pointed out recently [19], this can result in a period of late-time inflation which sets the relic density in a completely novel way. In both cases, a PT takes place in the early Universe from a $SU(2)_D$ symmetric vacuum in which the would-be-DM is massless, to a vacuum in which the dark gauge symmetry is broken and the DM is massive. The key point of our analysis is that the parameters setting the relic density also enter the effective potential determining the PT. As we will see, this allows us to find correlations between the GW signal and the DM properties.

This study is timely, as much work is being done on understanding GWs from cosmological PTs in anticipation of LISA [8], and follow-up proposals such as BBO [20]. In our analysis astrophysical foregrounds will be taken into account. These are mostly due to binaries of white dwarfs and are crucial for estimating the signal-to-noise ratio at future GW observatories [6, 7]. The paper is organized as follows. In Section 2, we present our DM model and its phenomenology. In Section 3, we calculate the GW signal arising from the PT for the standard and the classically scale invariant cases. We conclude in Section 4 by presenting a summary and outlook for this work. Appendix A is devoted to details concerning the effective potential, which determines the nature of the PT.

[1] CPT is the only SM discrete symmetry that is conserved.

2 DM as massive gauge bosons

2.1 The model

In this section we will describe the model and define notation. As mentioned in the introduction, we consider an extension of the SM with a dark $SU(2)_D$ gauge symmetry [13], under which all the SM particles are singlets. In addition to the dark gauge bosons $A^i_{D\mu}$ $(i = 1, 2, 3)$, the model has a dark scalar doublet, H_D, which carries no SM charges. Hence, the Lagrangian of the model is

$$\mathcal{L} = \mathcal{L}_{\rm SM} - \frac{1}{4} F_D \cdot F_D + (\mathcal{D}H_D)^\dagger (\mathcal{D}H_D) - \mu_2^2\, H_D^\dagger H_D - \lambda_2\, (H_D^\dagger H_D)^2 - \lambda_3\, H_D^\dagger H_D\, H^\dagger H\,, \quad (1)$$

where $\mathcal{L}_{\rm SM} \supset -\mu_1^2 H^\dagger H - \lambda_1 (H^\dagger H)^2$ and H is the SM scalar doublet. Here, F_D is the field strength tensor of the $SU(2)_D$ gauge symmetry and $\mathcal{D} = \partial + i g_D \tau^i \cdot A^i_D/2$ is the corresponding covariant derivative. We write scalar doublets as

$$H = \frac{1}{\sqrt{2}} \begin{pmatrix} G^2 + iG^3 \\ \phi + h + iG^1 \end{pmatrix}\,, \qquad\qquad H_D = \frac{1}{\sqrt{2}} \begin{pmatrix} G_D^2 + iG_D^3 \\ \eta + h_D + iG_D^1 \end{pmatrix}\,, \quad (2)$$

where ϕ and η are the classical field values breaking the electroweak and the $SU(2)_D$ symmetries, respectively. In addition, h, h_D, G^i and $G^i_D (i = 1, 2, 3)$ are the corresponding Higgs and Goldstone boson fields.

Symmetry breaking at tree level

In this case, the minimum of the potential associated with Eq. (1) is located at $(\phi, \eta) = (v_\phi, v_\eta)$, where $v_\phi = 246\,\text{GeV}$ and

$$\mu_1^2 = -\lambda_1\, v_\phi^2 - \frac{1}{2}\lambda_3\, v_\eta^2\,, \qquad\qquad \mu_2^2 = -\lambda_2 v_\eta^2 - \frac{1}{2}\lambda_3 v_\phi^2\,. \quad (3)$$

The mixing of the real scalars is captured by the usual angle

$$\tan 2\theta = \frac{\lambda_3\, v_\phi\, v_\eta}{\lambda_2\, v_\eta^2 \,-\, \lambda_1\, v_\phi^2}\,. \quad (4)$$

For convenience we commit a small abuse of notation, and from now on also label the mass eigenstates with h and h_D, where $m_h = 125\,\text{GeV}$. The mass eigenvalues are given by

$$m_h^2 \;=\; 2\,\lambda_1\, v_\phi^2\, \cos^2\theta \,+\, 2\,\lambda_2\, v_\eta^2\, \sin^2\theta \,-\, \lambda_3 v_\phi\, v_\eta\, \sin 2\theta\,, \quad (5)$$

$$m_{h_D}^2 \;=\; 2\,\lambda_1\, v_\phi^2\, \sin^2\theta \,+\, 2\,\lambda_2\, v_\eta^2\, \cos^2\theta \,+\, \lambda_3 v_\phi\, v_\eta\, \sin 2\theta\,. \quad (6)$$

All the dark gauge bosons obtain the mass, $m_A = g_D v_\eta/2$. In fact, they transform as a triplet under the accidental custodial $SO(3)$ symmetry. Thus, there are four parameters in the DM sector, which we take as m_A, g_D, θ and m_{h_D}.

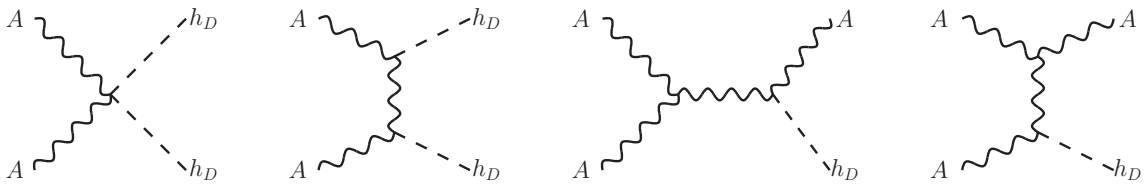

Figure 1: The dominant DM annihilation channels for $m_A \gg m_{h_D}$ and $\theta \ll 1$.

Radiatively-induced symmetry breaking

An alternative possibility is to consider a classically scale invariant realisation of this model [18, 19], where the mass terms in Eq. (1) are forbidden and symmetry breaking is achieved through radiative effects. This is known as the Coleman-Weinberg mechanism [21, 22]. We will focus on v_η at the TeV scale or above, in which case the the ϕ direction can be neglected for analysing the breaking of the $SU(2)_D$ symmetry. Under these assumptions, $\mathcal{L} \supset -\lambda_2 \eta^4/4$, where the coupling λ_2 is evaluated at a sliding scale given by the value of the η field. The running is obtained by integrating the corresponding β function, which gives

$$\lambda_2(\eta) \approx \frac{9\, g_D^4}{128\pi^2} \mathrm{Ln}\left(\frac{\eta}{\eta_0}\right) . \tag{7}$$

Here, we have neglected the contributions of λ_2 and λ_3 to the β function as well as the running of g_D. According to this, λ_2 becomes negative for field values below the integration constant η_0. This signals the breaking of the $SU(2)_D$ gauge symmetry. In fact, the minimization conditions on the corresponding potential (discussed in Appendix A.2), to leading order in λ_3, give $v_\eta = \eta_0 e^{-1/4}$ together with

$$m_{h_D}^2 = \frac{9\, g_D^4}{128\pi^2} v_\eta^2 \qquad \text{and} \qquad m_h^2 = -\lambda_3 v_\eta^2 . \tag{8}$$

Furthermore, electroweak symmetry breaking is triggered via the cross quartic coupling λ_3 so that $v_\phi = v_\eta \sqrt{-\lambda_3/(2\lambda_1)}$. Note that all this requires $\lambda_3 < 0$. As in the previous case, the dark gauge bosons obtain a mass $m_A = g_D v_\eta/2$. Notice also that, after accounting for $m_h = 125\,\mathrm{GeV}$ and $v_\phi = 246\,\mathrm{GeV}$, there are only two free parameters, which we choose as m_A and g_D. Before discussing DM production, we would like to emphasize that this scenario is not simply a limit of the previous case when μ_1 and μ_2 approach zero because here the breaking of the symmetry does not occur at tree level. (For a detailed discussion on such a limit, see [21].)

2.2 Relic density

We will consider two production regimes for the DM relic density: the standard freeze-out scenario and super-cool DM.[2] The latter only takes place for the classically scale invariant case, i.e. when the gauge symmetry is broken radiatively. Details are given in section 3.3. For the former case, we make the mild assumption that λ_3 and g_D are large enough so that

[2]Other production mechanism for this model have been discussed in [23].

DM was in thermal equilibrium with the SM fields in the Early Universe. Freeze-out leads to the observed dark matter abundance, $\Omega h^2 \simeq 0.12$, when the corresponding cross section is of the order $2.3 \times 10^{-26}\,\mathrm{cm}^3/\mathrm{s}$. This means that for given m_A, m_{h_D}, and θ, the relic density fixes the dark coupling g_D. We are interested in the regime in which $m_A > 2m_{h_D}$ so that DM (semi-)annihilates into dark Higgs bosons. We make the further simplifying assumption, $m_A \gg m_{h_D}$ and $\theta \ll 1$, so that the dominant annihilation channels are those shown in Fig. 1. In this regime the correct relic density is achieved for,

$$g_D \approx 0.9 \times \sqrt{\frac{m_A}{1\ \mathrm{TeV}}} \quad \text{and} \quad v_\eta \approx 2.2\,\mathrm{TeV} \times \sqrt{\frac{m_A}{1\ \mathrm{TeV}}}. \tag{9}$$

A more accurate determination can be achieved by numerically solving the Boltzmann equations. Given the uncertainties of the gravitational wave spectrum, however, the use of Eq. (9) is sufficient for our purposes.

2.3 Direct detection

The spin independent scattering cross-section of dark matter off nucleons is [13]

$$\sigma_{\mathrm{SI}} = \frac{g_D^4\, f^2\, m_N^4\, v_\eta^2}{64\pi\,(m_N + m_A)^2\, v_\phi^2} \left(\frac{1}{m_h^2} - \frac{1}{m_{h_D}^2}\right)^2 \sin^2 2\theta, \tag{10}$$

where m_N denotes the nucleon mass and $f \simeq 0.3$ is a constant that depends on the nucleon matrix element. Working in the limit $m_A \gg m_{h_D} \gg m_h$ and substituting Eq. (9) into σ_{SI}, one finds $\sigma_{\mathrm{SI}} \propto m_A \sin^2 2\theta$, i.e. with no further dependence on the other DM parameters. Then comparing to direct detection constraints — which also scale as $\sigma_{\mathrm{SI}}^{\mathrm{limit}} \propto m_{\mathrm{DM}}$ for $m_{\mathrm{DM}} \gtrsim 100$ GeV — we find current experiments such as Xenon1T demand $\theta \lesssim 0.1$ [24–26]. Future experiments such as LUX-Zepelin, will improve $\sigma_{\mathrm{SI}}^{\mathrm{limit}}$ by two orders of magnitude and therefore probe down to $\theta \approx 0.01$ [27–30].

3 Gravitational waves

3.1 Calculation of the spectrum

The first step is to derive the finite-temperature effective potential $V(\phi, \eta, T)$. We use well-known techniques of thermal field theory, the details are given in appendix A. We now briefly discuss the procedure used to calculate the gravitational wave spectrum resulting from a phase transition [8]. The crucial quantity is the $O(3)$ symmetric Euclidean action S_3. To calculate S_3, we numerically find the bubble profile by solving the associated equations of motion with the appropriate boundary conditions. Nucleation occurs at a temperature T_n when the bubble nucleation rate in the horizon volume becomes comparable to the Hubble parameter H. This happens when $S_3/T \approx 4\mathrm{Ln}(T/H)$ [31].[3] Having found T_n, it is trivial to find the latent heat normalised to the radiation density, α, and the timescale of the

[3]For the PTs studied below, we have checked $S_3/T_n < S_4$, where S_4 is the $O(4)$ symmetric action.

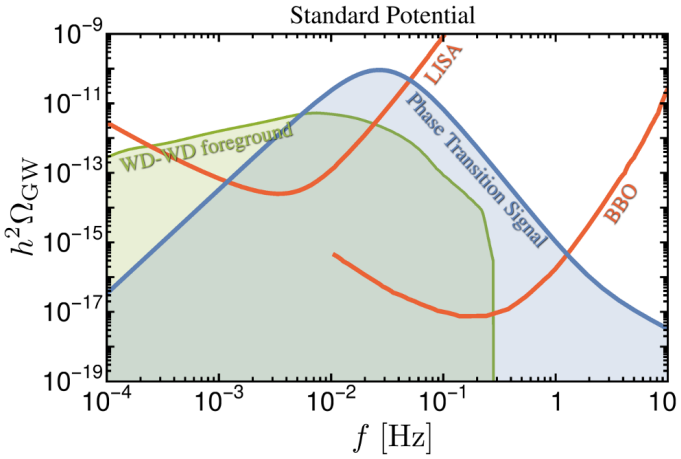

Dark Sector Parameters	m_A	3.0	TeV
	m_{h_D}	0.8	TeV
	v_η	0.9	TeV
	g_D	1.6	-
	θ	0.1	-
Phase Transition	T_n	0.5	TeV
	η_n	3.8	TeV
	α	0.4	-
	β/H	290	-
SNR	LISA	43	-
	LISA(FGL)	4.9	-
	BBO	10^6	-
	BBO(FGL)	10^4	-

Figure 2: An example of the gravitational wave spectrum when the symmetry breaking occurs at tree level, together with the white-dwarf white-dwarf binary foreground, and LISA and BBO sensitivity curves. Here we assume $v_w = 1$.

transition $\beta \equiv -\frac{d}{dt}(S_3/T)\big|_{T_n}$. For the strongest of PTs, we expect the wall velocity to be close to luminal, $v_{\rm w} \simeq 1$. This is because the mean field potential typically satisfies,

$$\overline{V} = V(\phi_n, \eta_n, T=0) - V(\phi_0, \eta_0, T=0) + \frac{T^2}{24}\left(\sum_{\rm bosons}\left[m_b^2(\phi_n,\eta_n) - m_b^2(\phi_0,\eta_0)\right] + \frac{1}{2}\sum_{\rm fermions}\left[m_f^2(\phi_n,\eta_n) - m_f^2(\phi_0,\eta_0)\right]\right) < 0, \tag{11}$$

where (ϕ_n, η_n) is the true and (ϕ_0, η_0) the false vacuum at T_n. This is the Bodeker-Moore (BM) criterion [32]. We shall make clear on our plots where the BM criterion holds and what we assume regarding v_w when it does not.

Even when the BM criterion holds, however, the wall is not expected to runaway with $\gamma \to \infty$, due to the transition radiation effect from the gauge bosons [33]. Therefore, provided the gauge boson population has not been overly diluted by false vacuum inflation, energy released in the transition is transfered to the radiation bath, in which sound waves [34–36] and magnetohydrodynamic turbulence [37, 38], rather than the bubble wall collisions directly [39–44], lead to a gravitational wave signal. Determining α and β allows us to find the spectral function of gravitational waves,

$$h^2\Omega_{\rm GW}(f) \equiv h^2 \frac{f}{\rho_c}\frac{d\rho_{\rm GW}}{df}, \tag{12}$$

where ρ_c is the critical density, and $d\rho_{GW}/df$ is calculated using the approximate formulas from the literature [8,45]. An example of the spectrum is shown in Fig. 2. We use estimated sensitivity of the gravitational wave detectors to stochastic backgrounds, $h^2\Omega_{\rm sens}(f)$, for LISA [8] and BBO [20]. The signal-to-noise ratio can be estimated using [8]

$${\rm SNR} = \sqrt{t_{\rm obs}\int\left[\frac{h^2\Omega_{\rm GW}(f)}{h^2\Omega_{\rm sens}(f)}\right]^2 df}, \tag{13}$$

where $t_{\rm obs}$ is the time of observation in years. We assume $t_{\rm obs} = 5$ throughout.

Confusion noise from astrophysical foregrounds may be an issue at these frequencies. We shall compare to some estimates of the unresolvable components given in the literature. The ensemble of white dwarf - white dwarf (WD-WD) binaries are thought to be the dominant source of this foreground, exceeding the unresolvable neutron star - neutron star (NS-NS) foreground [46,47]. In this work we restrict ourselves to the foreground from the extragalactic WD-WD ensemble and use the central value given in [46]. We make this choice because, in contrast to the extragalactic ensemble, it is thought the WD-WD Galactic foreground [48–50] can be subtracted [51,52]. The continuous extragalactic NS-NS foreground extends to higher frequencies in the BBO band, however, it is thought that this can also be subtracted [53,54]. We also adopt an alternative, foreground-limited, estimate of the signal-to-noise ratio

$$\mathrm{SNR}_{\rm FGL} = \sqrt{t_{\rm obs} \int \left[\frac{h^2\Omega_{\rm GW}(f)}{h^2\Omega_{\rm sens}(f) + h^2\Omega_{\rm FG}(f)} \right]^2 df}, \tag{14}$$

in which we attempt to naively capture the degradation of the sensitivity once the foreground, $h^2\Omega_{\rm FG}(f)$, is taken into account. The aim of introducing Eq. (14) is to be able to roughly capture, in a single number, whether the signal extends above the sensitivity and foreground estimate. Whether such a PT signal could actually be separated from the astrophysical foreground depends, of course, on a myriad of factors, e.g. the robustness of the estimates of the amplitudes and spectral shapes of the signal and foreground, together with the confidence in our knowledge of the instrumental noise. These are topics worthy of further study, but we will not attempt to do them justice here. Nevertheless, we would like to remark that the LISA $\mathrm{SNR}_{\rm FGL}$ value associated to the spectrum of Fig. 2 clearly illustrates the importance of astrophysical foregrounds, even though they are often ignored in similar studies.

3.2 Symmetry breaking at tree level

As discussed above, in this case the DM production proceeds via the standard freeze-out mechanism. Interesting for us is the regime with a large g_D, as this will lead to a strong phase transition. This pushes us to large m_A and v_η, see Eq. (9), and the dark phase transition will generally occur prior to the EW one. Thus the task of studying the phase transition reduces to one dimension in field space. We have seen an example of the gravitational wave spectrum, together with the dominant foreground, in Fig. 2. We have also fixed θ to 0.1 and 0.01 (motivated by present and future direct detection constraints), scanned over the parameters m_A and m_{h_D} and calculated the GW signal. The result is shown in Fig. 3.

The plot can be understood as follows. A larger DM mass, m_A, requires a larger gauge coupling in order to return the observed DM density. This results in a stronger phase transition from the one-loop effects of the gauge bosons. Similarly, in analogy with the SM, a lighter dark Higgs — corresponding to a smaller quartic λ_2 — also leads to a stronger transition because the broken phase minimum is shallower. Nevertheless, for particularly large values of m_A/m_{h_D}, the one-loop effects can raise the broken phase minimum too far, resulting in the Universe becoming stuck in the symmetric phase. The latter can either be a false or true minimum, corresponding to the orange and red shaded regions of the figure respectively. We expect the allowed parameter space to be increased somewhat, into the orange region, if S_4 nucleation at lower temperatures were to be taken into account.

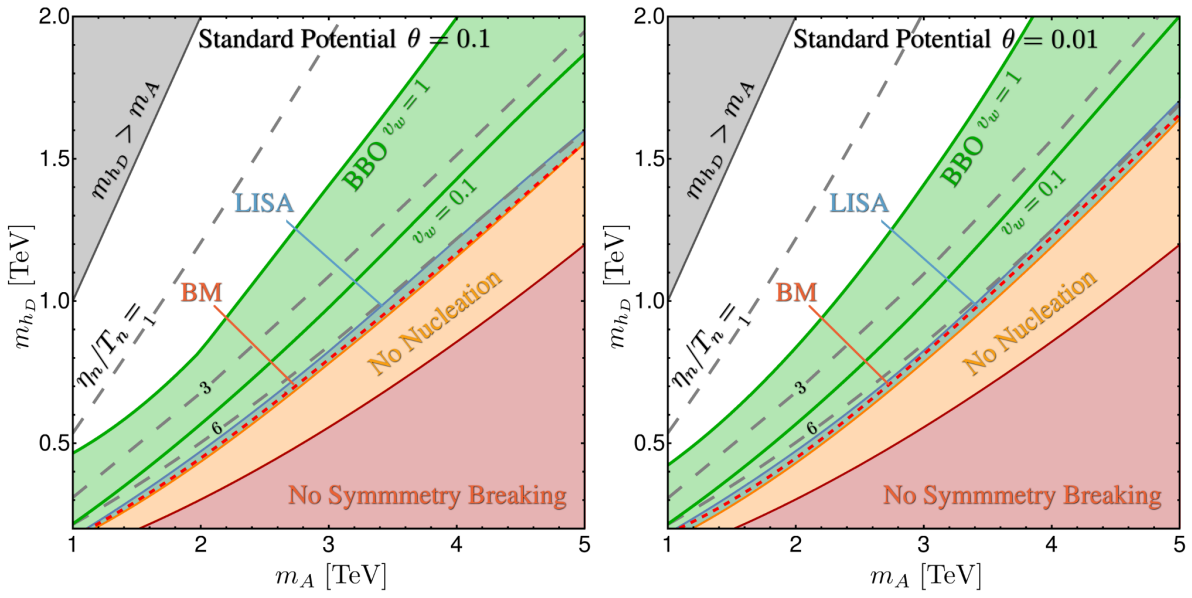

Figure 3: The parameter space returning a significant BBO or LISA signal, SNR > 5, when the symmetry breaking occurs at tree level (standard potential). For LISA we assume $v_w = 1$ as the BM criterion is fulfilled roughly in this region. For BBO we show contours assuming $v_w = 0.1$ and 1. Only the strongest transitions, close to the point at which no transition occurs at all, can be probed by LISA in this case. In contrast BBO can probe a substantial fraction of the parameter space with a strong first order phase transition. Here we show the SNR with no foreground. If the foreground is included the BBO area remains practically unchanged, while the already small LISA area is approximately halved.

3.3 Radiatively-induced symmetry breaking: standard freeze-out and super-cool DM

Another possibility is to impose classical scale invariance on the theory, as explained above. This scenario with our field content has been studied in [18, 19]. Such a potential typically exhibits a large amount of supercooling [55–73]. This is because, lacking a mass term, the $T = 0$ potential is very flat in field space. Furthermore, the positive thermal corrections from the gauge bosons will lead to a barrier being present for any finite T. Somewhat counter intuitively, a smaller g_D actually leads to more supercooling because the $T = 0$ potential becomes shallower, as shown in Fig. 4. The thermal barrier also becomes smaller, but the shallower potential ends up being the more important effect.

Of importance for the DM relic density in this scenario, is not just the DM annihilation cross section, but also the details of the phase transition. In particular the nucleation temperature, T_n, the temperature when inflation starts, $T_{\rm infl}$, and the reheating temperature, $T_{\rm RH}$. The latter two quantities are calculated following the methods in [19].

Furthermore, due to the large amount of supercooling, the PT may actually not take place before the temperature falls to $T \sim \Lambda_{\rm QCD}$. In this particular case, the $SU(2)_D$ PT is induced by QCD effects [55, 57, 69, 72]. Our calculation of the nucleation temperature, ignoring the QCD trigger for now, is shown in Fig. 4.

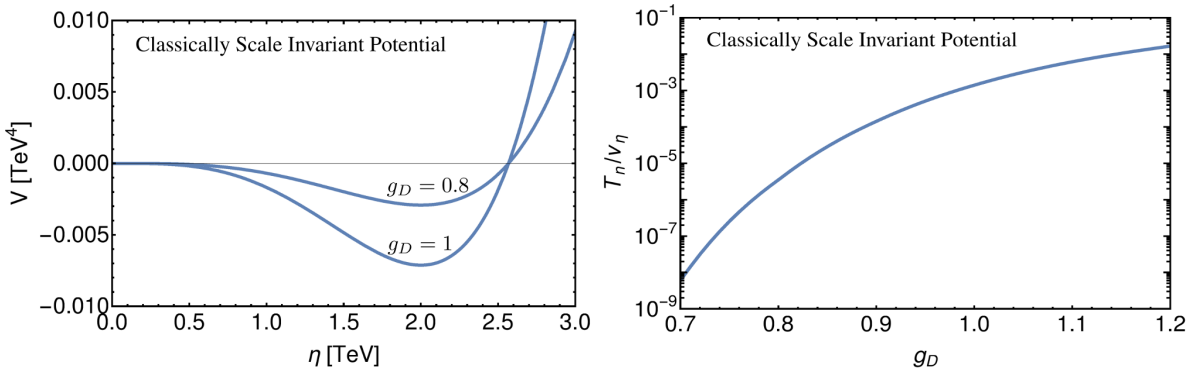

Figure 4: *Left:* the classically scale invariant potential ($T = 0$) with $v_\eta = 2$ TeV and two choices of the gauge coupling. *Right:* the nucleation temperature as a function of the gauge coupling in the classically scale invariant case, for a fixed nucleation condition $S_3/T = 142$, and ignoring QCD effects.

As a result, in the classical invariance scenario two distinct possibilities for the relic density can play out.

- **Regime (i): standard freeze-out.**

  (ia). $T_n > \Lambda_{\rm QCD}$. There is a large thermal abundance of massive gauge bosons after the phase transition, i.e. if $T_{\rm RH}/m_A$ and g_D are large enough to bring (or keep) the gauge bosons in thermal equilibrium. Therefore, following the phase transition, the relic density is set through the usual freeze-out mechanism. Typically this occurs for gauge couplings $g_D \sim 1$ and $m_A \gtrsim 1.2$ TeV.

  (ib). $T_n < \Lambda_{\rm QCD}$. This is similar to above, except the sequence of PTs is switched. Most of the parameter space corresponding to this regime has been ruled out by direct detection [19], except for the mass range 0.9 TeV $\lesssim m_A \lesssim$ 1.2 TeV.

- **Regime (ii): super-cool DM.**

  (iia). $T_n > \Lambda_{\rm QCD}$. There is sufficient supercooling for a period of late time inflation to take place. Before the phase transition, the gauge bosons are massless and have a large abundance. This abundance is diluted away by the period of late time inflation. The relic density in principle consists of the diluted, now super-cool, population of gauge bosons, together with an additional sub-thermal component created through scatterings after reheating. Numerically, however, we find the sub-thermal population is negligible in the parameter space corresponding to this regime, leaving the DM relic abundance set by the super-cool population of gauge bosons. The parameter space here corresponds to $g_D \sim 1$ and $m_A \gtrsim 370$ TeV.

  (iib). $T_n < \Lambda_{\rm QCD}$. This is again conceptually similar to above except the PTs are switched. The sub-thermal DM population is now important for a large range of the parameter space, which corresponds to $g_D \lesssim 1$ and $m_A \lesssim 370$ TeV.

In all regimes, once the relic density constraint is used, we are left with one free parameter which we take to be m_A. Here we wish to point out, supported by our calculations, that

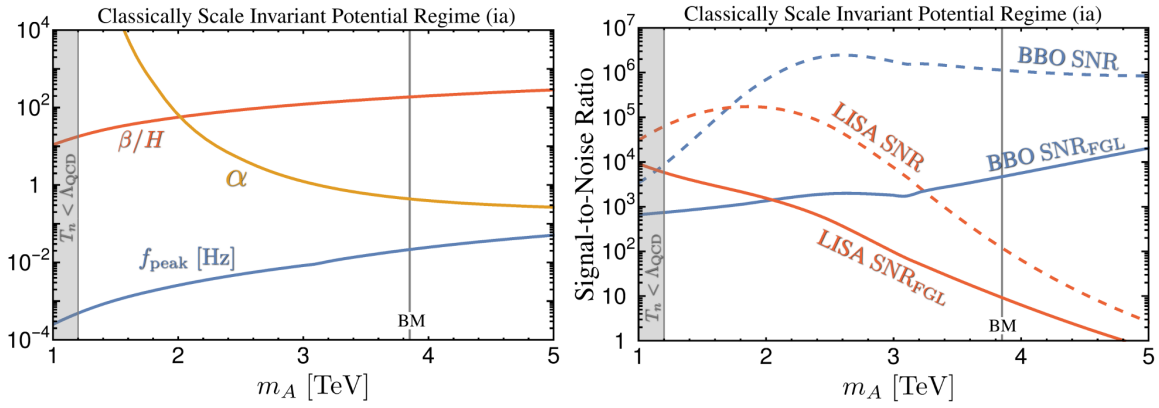

Figure 5: *Left:* the key phase transition parameters in regime (ia) of the scale invariant case. *Right:* The SNR for LISA and BBO. The Bodeker-Moore criterion, showing $v_w \simeq 1$, is satisfied for $m_A \lesssim 3.8$ TeV. Above this we still assume $v_w \approx 1$, though it could be lower, which would reduce the SNR.

large portions of the parameter space of the classically scale invariant scenario can be probed through GW observatories. We shall now discuss the GW signal in each regime in turn.

Regime (ia)

The GW signal in this regime has previously been discussed in [18]. Here we provide our own — updated and expanded — calculation for completeness. For simplicity we assume the spectrum is given by the sum of the sound wave and turbulent contributions over the entire regime. Below $m_A \lesssim 1.8$ TeV this may not be a good approximation, as the initial population of gauge bosons is reduced by late inflation by a factor > 100, meaning the plasma contribution may be negligible. Nevertheless, the PT is strong enough for $m_A \lesssim 1.8$ TeV to be observable even with the scalar field contribution. The key phase transition parameters are shown in Fig. 5, together with the foreground-free and foreground-limited signal-to-noise ratios. Note reheating is efficient in this regime: there is no period of matter domination immediately following the PT, as the decay rate of the inflaton is sufficiently large, $\Gamma > H$.

As can be seen from Fig. 5, LISA can probe DM masses in this regime up to $m_A \sim 4$ TeV, even in the presence of the WD-WD foreground. This is competitive with projections for future direct detection experiments [27–30], which can probe up to $m_A \sim 2$ TeV [19]. (The current direct detection constraint demands $m_A \gtrsim 0.9$ TeV [19, 24–26].) The BBO proposal could test the entire parameter space shown here, well into what corresponds to the neutrino floor for direct detection experiments. Note for $m_A \lesssim 1.2$ TeV we find ourselves in regime (ib), which is discussed below.

Regime (iia)

Following the methods in [19], we find this regime corresponds to parameters $g_D \approx 1$ and $m_A \gtrsim 370$ TeV. Notice that these DM masses are well above the usual unitarity constraint from the thermal freeze-out of DM [74, 75], which does not take place here. Numerically the

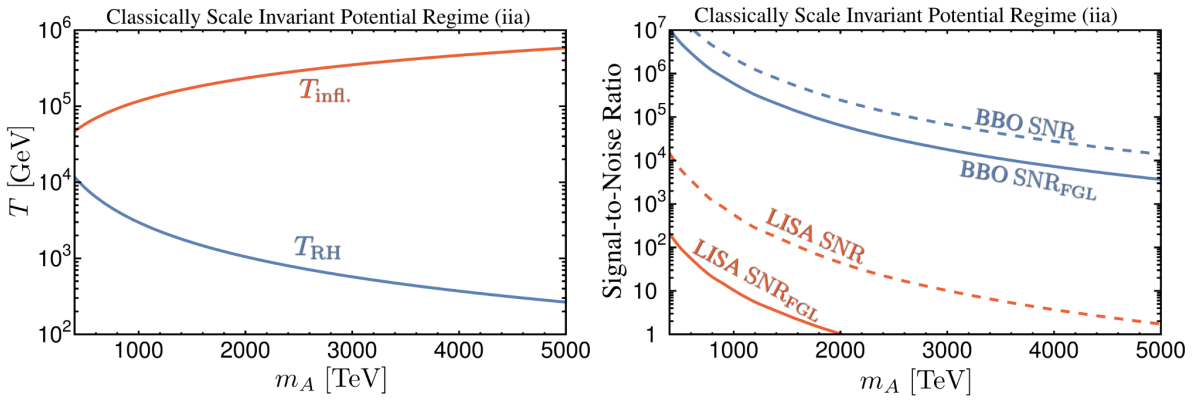

Figure 6: *Left:* The temperature when inflation starts, $T_{\rm infl}$, and the reheating temperature, T_{RH}, in regime (iia). The ratio $(T_{\rm infl}/T_{\rm RH})$ determines the amount of additional redshifting of the signal due to the matter dominated reheating period following the PT. *Right:* the detectability of the GW signal in regime (iia). Here the BM criterion holds over the entire range.

required g_D grows slowly, from $g_D = 0.95$ for $m_A = 370$ TeV, to $g_D = 1.02$ for $m_A = 10000$ TeV. Our calculation of $T_{\rm RH}$ and $T_{\rm infl}$ is shown in Fig. 6. In this regime, reheating is inefficient following the PT, thus $T_{\rm RH} \neq T_{\rm infl}$. Indeed, there is a period of matter domination following the PT, as η oscillates about the minimum of its potential. More precisely, the ratio of scale factors between the PT and the end of reheating is given by

$$\frac{a_{\rm PT}}{a_{\rm RH}} = \left(\frac{T_{\rm RH}}{T_{\rm infl}}\right)^{4/3}. \tag{15}$$

This leads to greater expansion of the Universe between the PT and today, suppressing the signal, and redshifting the frequency further than would otherwise be the case.

The GW spectrum is determined in the following way. First of all, as the thermal plasma has been diluted away by the time of the PT, the scalar field configuration — and not sound waves or turbulence — is the source of the signal. It has been suggested that the oscillations of the scalar field after the PT may increase both that peak frequency and energy density of the GW signal by an order of magnitude [76]. We choose to remain conservative, however, and base our spectrum on [8]. Once the Universe enters the late inflationary stage at $T_{\rm infl}$, the energy density remains constant until the plasma temperature reaches T_n, and so the Hubble scales at both temperature are the same $H(T_n) = H(T_{\rm infl})$. Taken together, β and $H \sim T_{\rm infl}^2/M_{\rm Pl}$ set the initial frequency of the GW signal. We then redshift this value to $T_{\rm RH}$ when the Universe once again enters a radiation dominated phase. The redshifting from $T_{\rm RH}$ to today then follows the standard calculation [8]. Taking all this, together with Eq. (15) into account, the peak frequency is given by

$$f_{\rm peak}^{(iia)} = 16.5\,\mu{\rm Hz}\left(\frac{T_{\rm RH}}{T_{\rm infl}}\right)^{1/3}\left(\frac{f_*}{\beta}\right)\left(\frac{\beta}{H}\right)\left(\frac{T_{\rm infl}}{100\,{\rm GeV}}\right)\left(\frac{g_*}{100}\right)^{1/6}, \tag{16}$$

where g_* counts the effective degrees of freedom contributing to the radiation density, and $f_*/\beta = 0.62/(1.8 - 0.1v_w + v_w^2)$ is taken from simulations [44]. The amplitude of the spectrum

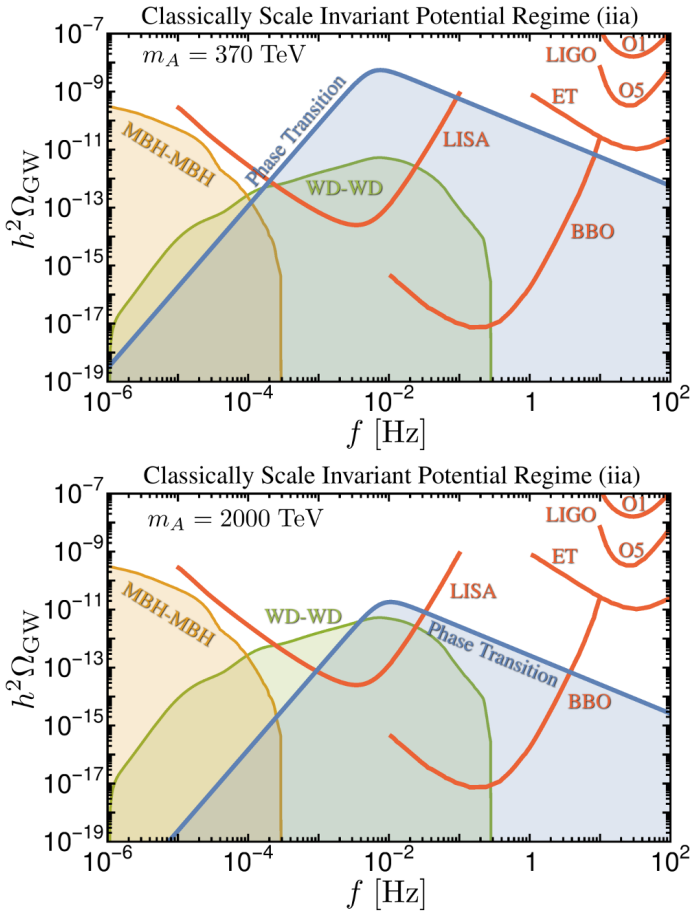

Dark Sector Parameters	m_A	370	TeV
	m_{h_D}	59	TeV
	v_η	780	TeV
	g_D	0.95	-
	θ	10^{-9}	-
Phase Transition	T_n	2.6	GeV
	$T_{\rm infl.}$	43	TeV
	$T_{\rm RH}$	13	TeV
	η_n	$\simeq v_\eta$	-
	α	10^{16}	-
	β/H	6.7	-
SNR	LISA	10^4	-
	LISA(FGL)	270	-
	BBO	10^8	-
	BBO(FGL)	10^7	-

Dark Sector Parameters	m_A	2000	TeV
	m_{h_D}	330	TeV
	v_η	4100	TeV
	g_D	0.98	-
	θ	10^{-11}	-
Phase Transition	T_n	32	GeV
	$T_{\rm infl.}$	230	TeV
	$T_{\rm RH}$	1.0	TeV
	η_n	$\simeq v_\eta$	-
	α	10^{15}	-
	β/H	7.1	-
SNR	LISA	44	-
	LISA(FGL)	1.0	-
	BBO	10^5	-
	BBO(FGL)	10^5	-

Figure 7: Examples of GW spectra in regime (iia). Although $\alpha \gg 1$, and β/H is similar for both phase transitions, the period of matter domination after the PT is longer for larger m_A, leading to a suppressed signal. For purposes of illustration we also include the unresolvable foreground from black hole binaries with masses $10^2 M_\odot - 10^{10} M_\odot$ (MBH-MBH) [47].

is also suppressed with respect to the case with no early period of matter domination,

$$\Omega_{\rm GW} \to \left(\frac{T_{\rm RH}}{T_{\rm infl}}\right)^{4/3} \Omega_{\rm GW}, \tag{17}$$

because $\Omega_{\rm GW} = \rho_{\rm GW}/\rho_c \propto a^0$, (a^{-1}) in a radiation (matter) dominated Universe. Accounting for these factors, we find the GW spectra and summarise their detectability in Fig. 6. Examples of the spectra are shown in Fig. 7. Notice that for these large masses, the frequency of the gravitational waves extends well above 1 Hz, motivating us to compare our signal against sensitivity curves from current and future LIGO configurations O1 and O5 [54] and the Einstein Telescope (ET) [77].

Regimes (ib) and (iib)

The $SU(2)_D$ phase transition occurs after QCD confinement. The QCD phase transition occurs with six massless quarks and is first order [78,79]. There is a chance this could lead to

an observable GW signal [9,69]. We cannot, however, use our techniques above to accurately calculate the phase transition parameters, α and β for the QCD phase transition [69]. Most likely a lattice study is required in order to more carefully explore this possibility. Alternative techniques have been pursued in [67, 70].

We now turn to the details of the $SU(2)_D$ phase transition following shortly after the QCD one. The quark condensate formed after chiral symmetry breaking leads to a tadpole term and hence a VEV for the EW Higgs. This in turn leads to a mass term for η through the cross-quartic. Provided $3m_A^2 \gtrsim 2m_h^2$, which corresponds to our regime of interest, the thermal barrier from the gauge bosons is still large enough to prevent immediate $SU(2)_D$ breaking. Instead, a first order phase transition occurs just before the barrier disappears at $T \sim m_h \Lambda_{\rm QCD}/m_A$. As can be checked numerically, the non-zero mass term for η means this phase transition now occurs with a very large β, and does not lead to an observable gravitational wave signal.

4 Discussion and Conclusion

We have explored the possibility of spin-one DM from a hidden $SU(2)_D$ gauge group. The stability of DM is elegantly assured through an accidental custodial symmetry. Given the massive vector bosons, unitarity demands that the $SU(2)_D$ be broken through the Higgs mechanism. This implies a phase transition or crossover occurred in the dark sector, i.e. the symmetry was initially unbroken at high temperatures. A strong phase transition will result in gravitational waves possibly detectable at future gravitational wave observatories.

In this scenario the $SU(2)_D$ gauge coupling plays a crucial role in determining the relic abundance through freeze-out or late-time inflation. The same gauge coupling controls both the scattering cross-section and the thermal effects of the gauge bosons relevant for the phase transition. The model is therefore well suited as a case study for the sensitivity of future gravitational wave observatories to phase transitions in DM sectors.

We studied both tree level and radiatively-induced symmetry breaking. After finding the resulting gravitational wave spectra we identified parameter space which can be probed by LISA and BBO. As is known from previous studies, only limited parameter space of standard polynomial type potentials can be tested by LISA. The prospects improve for the classically scale invariant scenario. In this case, LISA is competitive with future direct detection experiments in the freeze-out regime and can probe the new regime of super-cool DM, which is inaccessible to direct and indirect detection. Nevertheless, a conclusive test could only be performed by a more powerful observatory such as BBO.

We saw how foregrounds, which have so far been largely ignored in phase transition studies, apart from in [6, 7], can be taken into account in the estimates of the signal-to-noise ratio. Our results should be taken as indicative; we expect updated estimates of foregrounds to become available as our knowledge of the binary populations improves. More sophisticated studies, taking into account the precise capability of the LISA and eventually BBO spacecraft are required. Simulations of sound waves in the plasma for $\alpha > 0.1$ should also be performed. Only then will it be possible to conclusively rule out models from their implied gravitational wave signals using future LISA and BBO data. A positive signal at LISA — which requires a very strong phase transition — would most likely point toward exotic new physics at the

TeV scale such as the close-to-conformal potential studied here.

Acknowledgements

The authors thank D. Teresi for helpful correspondence regarding super-cool DM. We thank J. R. Espinosa and T. Konstandin for clarifying discussion. C.G.C. is supported by the ERC Starting Grant NewAve (638528).

A The effective potential

A.1 Symmetry breaking at tree level

The full effective potential is composed of four pieces

$$V(\phi,\eta,T) = V_{\rm tree}(\phi,\eta) + V_1^0(\phi,\eta) + V_1^{\rm c.t}(\phi,\eta) + V_1^T(\phi,\eta,T)\,. \tag{18}$$

The tree-level piece

This directly follows from Eq. (1) and it is given by

$$V_{\rm tree}(\phi,\eta) = \frac{\mu_1^2}{2}\phi^2 + \frac{\lambda_1}{4}\phi^4 + \frac{\mu_2^2}{2}\eta^2 + \frac{\lambda_2}{4}\eta^4 + \frac{\lambda_3}{4}\eta^2\phi^2. \tag{19}$$

Coleman-Weinberg potential at zero temperature

Knowing the field dependent masses, $m_i(\phi,\eta)$, in the Laudau gauge the one-loop $T=0$ contribution is given by

$$V_1^0(\phi,\eta) = \sum_i \frac{g_i(-1)^F}{64\pi^2} m_i^4(\phi,\eta)\left(\mathrm{Ln}\left[\frac{m_i^2(\phi,\eta)}{\mu^2}\right] - C_i\right)\,, \tag{20}$$

where μ is the $\overline{\rm MS}$ renormalization scale and $g_i = \{1,3,6,12,1,9,3,3\}$ for the $h,\ Z,\ W^\pm,\ t,\ \eta,\ A,$ $G,\ G^D$. In addition, $C_i = 5/2$ for gauge bosons and $C_i = 3/2$ otherwise. Finally, $F = 0$ (1) for bosons (fermions).

The masses as a function of the scalar field values for the fermions and gauge bosons of the SM are

$$m_Z^2(\phi,\eta) = \frac{1}{4}(g_2^2+g_Y^2)\phi^2\,, \qquad m_W^2(\phi,\eta) = \frac{1}{4}g_Y^2\phi^2\,, \qquad m_t^2(\phi,\eta) = \frac{1}{2}y_t^2\phi^2\,. \tag{21}$$

Similarly, for the dark gauge bosons $m_A^2(\phi,\eta) = g_D^2\eta^2/4$. Due to the coupling λ_3 in Eq. (1), the scalar sectors mix with each other and the masses for the real scalar fields entering in Eq. (29) are the eigenvalues of the matrix

$$m^2_{\rm Higgs} \;=\; \begin{pmatrix} \mu_1^2 + 3\lambda_1\phi^2 + \frac{1}{2}\lambda_3\eta^2 & \lambda_3\,\phi\eta \\ \lambda_3\,\phi\eta & \mu_2^2 + 3\lambda_2\eta^2 + \frac{1}{2}\lambda_3\phi^2 \end{pmatrix}\,. \tag{22}$$

In spite of this, the Goldstone bosons *do not* mix at tree level. In fact, in the Landau gauge, their masses are given by

$$m^2_G(\phi,\eta) = \mu_1^2 + \lambda_1\phi^2 + \frac{1}{2}\lambda_3\eta^2\,, \tag{23}$$

$$m^2_{G_D}(\phi,\eta) = \mu_2^2 + \lambda_2\eta^2 + \frac{1}{2}\lambda_3\phi^2\,, \tag{24}$$

which vanish at $(\phi,\eta)=(v_\phi,v_\eta)$, as follows from Eqs. (3).

The counter-term potential

The counter terms to the potential in Eq. (29) are

$$V_1^{\rm c.t}(\phi,\eta) = \frac{\delta\mu_1^2}{2}\phi^2 + \frac{\delta\lambda_1}{4}\phi^4 + \frac{\delta\mu_2^2}{2}\eta^2 + \frac{\delta\lambda_2}{4}\eta^4 + \frac{\delta\lambda_3}{4}\eta^2\phi^2. \tag{25}$$

By demanding no changes to the masses and VEVs of the scalars from their tree level values, that is, by imposing

$$\partial_{\phi,\eta}(V_1^0 + V_1^{\rm c.t})\Big|_{(\phi,\eta)=(v_\phi,v_\eta)} = 0\,, \tag{26}$$

$$\partial_{\phi,\eta}\partial_{\phi,\eta}(V_1^0 + V_1^{\rm c.t})\Big|_{(\phi,\eta)=(v_\phi,v_\eta)} = 0\,, \tag{27}$$

$$\tag{28}$$

we calculate the couplings in Eq. (25). Moreover, we find[4]

$$V_1^0(\phi,\eta) + V_1^{\rm c.t}(\phi,\eta) = \sum_i \frac{g_i(-1)^F}{64\pi^2}\left\{ m_i^4(h,\eta)\left(\mathrm{Ln}\left[\frac{m_i^2(\phi,\eta)}{m_i^2(v_\phi,v_\eta)}\right] - \frac{3}{2}\right) + 2m_i^2(\phi,\eta)m_i^2(v_\phi,v_\eta)\right\} + \mathcal{O}(\lambda_3^2)\,. \tag{29}$$

In this equation, the prescription for the scalars $m_i^2(\phi,\eta)$ is the following. They are the eigenvalues of the mass matrix in Eq. (22), ordered in such way that

$$m_\pm^2(0,0) = \mathcal{F}_\pm(\mu_1^2,\mu_2^2) \qquad \text{and} \qquad m_\pm^2(v_\phi,v_\eta) = \mathcal{F}_\pm(m_\phi^2,m_\eta^2)\,, \tag{30}$$

where

$$\mathcal{F}_\pm(a,b) = \frac{1}{2}\left(a+b \pm (a-b)\mathrm{sgn}(|a|-|b|)\right)\,. \tag{31}$$

Notice that $\Sigma_\pm\mathcal{F}_\pm(a,b) = a+b$ and that, when a and b are both positive (negative), $\mathcal{F}_+(a,b)$ is the maximum (minimum) of them.

[4] There is a subtle issue for the contribution of the Goldstone bosons to Eq. (29). As explained above, their tree-level masses vanish at (v_ϕ,v_η) leading to an infrared divergence in Eq. (29). Such a divergence is spurious [80] and disappears after the one-loop contributions to the Goldstone-boson self-energies are accounted for. Neglecting any possible mixing effect due to non-vanishing λ_3, the latter can be calculated by means of $\delta m^2_G(\phi,\eta) = (1/2)\partial^2 V_1^{(0)}/\partial^2\phi$ and $\delta m^2_{G_D}(\phi,\eta) = (1/2)\partial^2 V_1^{(0)}/\partial^2\eta$.

Finite-temperature potential

The one-loop finite T contribution is given by

$$V_1^T(\phi,T) = \sum_i \frac{g_i(-1)^F T^4}{2\pi^2} \times \int_0^\infty y^2 \,\mathrm{Ln}\left(1-(-1)^F \mathrm{Exp}\left[-\sqrt{y^2+m_i^2(h,\eta)/T^2}\right]\right) dy. \tag{32}$$

In order to take into account the resummation of the Matsubara zero modes one includes the daisy term

$$V_{\rm Daisy}(\phi,T) = \sum_i \frac{\bar{g}_i T}{12\pi}\Big\{\left[m_i^2(\phi,\eta)\right]^{3/2} - \left[m_i^2(\phi,\eta)+\Pi_i(T)\right]^{3/2}\Big\} \tag{33}$$

where the sum runs only over scalars and the longitudinal degrees of freedom of the vector bosons, i.e $\bar{g}_i \equiv \{1,1,1,2,1,3,3,3\}$ for $h,\ Z,\ \gamma,\ W^\pm,\ \eta,\ A,\ G,\ G_D$. Here the thermal masses are given by [81]

$$\Pi_{\rm Higgs} = \begin{pmatrix} \frac{1}{2}\lambda_1 + \frac{1}{6}\lambda_3 + \frac{3}{16}g_2^2 + \frac{1}{16}g_Y^2 + \frac{1}{4}y_t^2 & 0 \\ 0 & \frac{1}{2}\lambda_2 + \frac{1}{6}\lambda_3 + \frac{3}{16}g_D^2 \end{pmatrix} T^2\,, \tag{34}$$

$$\Pi_G = \left(\frac{1}{2}\lambda_1 + \frac{1}{6}\lambda_3 + \frac{3}{16}g_2^2 + \frac{1}{16}g_Y^2 + \frac{1}{4}y_t^2\right) T^2, \tag{35}$$

$$\Pi_{G_D} = \left(\frac{1}{2}\lambda_2 + \frac{1}{6}\lambda_3 + \frac{3}{16}g_D^2\right) T^2\,, \tag{36}$$

$$\Pi_{Z/\gamma} = \begin{pmatrix} \left(\frac{5}{6}+\frac{n_f}{3}\right) g_2^2 & 0 \\ 0 & \left(\frac{1}{6}+\frac{5n_f}{9}\right) g_Y^2 \end{pmatrix} T^2\,, \tag{37}$$

$$\Pi_W = \left(\frac{5}{6}+\frac{n_f}{3}\right) g_2^2 T^2, \tag{38}$$

$$\Pi_A = \frac{5}{6} g_D^2 T^2, \tag{39}$$

where $n_f = 3$ is the number of fermionic families with $SU(2)\times U(1)$ charge. Note for the scalars and the Z/γ, the prescription here is that $m_i^2(\phi,\eta)$ represents the relevant eigenvalue of the zero temperature mass matrix and $m_i^2(\phi,\eta)+\Pi_i(T)$ the relevant eigenvalue of the zero temperature mass matrix with the thermal masses added along the diagonal. This means the Z and γ mix at finite temperature. To avoid spurious contributions to the thermal masses from the $SU(2)_D$ gauge bosons at large field values, we cut off the g_D contributions with a factor $(m_A/T)^2 K_2(m_A/T)/2$, where $K_2(x)$ is the modified Bessel function of the second kind of order two.

A.2 Classically Scale Invariant Potential

As explained in the text, in this case we have radiative symmetry breaking and the potential at one loop becomes [21, 22, 18, 19]

$$V_1^0(\eta) \simeq \frac{9 g_D^4 \eta^4}{512\pi^2} \left(\mathrm{Ln}\left[\frac{\eta}{v_\eta}\right] - \frac{1}{4} \right), \tag{40}$$

where the ϕ direction plays a completely negligible role in the area of parameter space in which we shall be interested. (The EW symmetry is broken by the induced mass term, $\lambda_3 v_\eta^2/2$, from the cross quartic.) The thermal effects are dominated by the gauge bosons. Thus the effective potential is well approximated by Eq. (40), together with the one-loop thermal, Eq. (32), and daisy terms, Eq. (33), for the $SU(2)_D$ gauge bosons.

References

[1] G. Bertone, D. Hooper, and J. Silk, "*Particle dark matter: Evidence, candidates and constraints*," Phys. Rept. **405** (2005) 279–390, arXiv:hep-ph/0404175.

[2] F. Kahlhoefer, "*Review of LHC Dark Matter Searches*," Int. J. Mod. Phys. **A 32** (2017) no. 13, 1730006, arXiv:1702.02430.

[3] J. M. Gaskins, "*A review of indirect searches for particle dark matter*," Contemp. Phys. **57** (2016) no. 4, 496–525, arXiv:1604.00014.

[4] T. Marrodán Undagoitia and L. Rauch, "*Dark matter direct-detection experiments*," J. Phys. **G 43** (2016) no. 1, 013001, arXiv:1509.08767.

[5] E. Witten, "*Cosmic Separation of Phases*," Phys. Rev. **D 30** (1984) 272–285.

[6] C. J. Hogan, "*Gravitational radiation from cosmological phase transitions*," Mon. Not. Roy. Astron. Soc. **218** (1986) 629–636.

[7] C. Grojean and G. Servant, "*Gravitational Waves from Phase Transitions at the Electroweak Scale and Beyond*," Phys. Rev. **D 75** (2007) 043507, arXiv:hep-ph/0607107.

[8] C. Caprini *et al.*, "*Science with the space-based interferometer eLISA. II: Gravitational waves from cosmological phase transitions*," JCAP **1604** (2016) no. 04, 001, arXiv:1512.06239.

[9] P. Schwaller, "*Gravitational Waves from a Dark Phase Transition*," Phys. Rev. Lett. **115** (2015) no. 18, 181101, arXiv:1504.07263.

[10] I. Baldes, "*Gravitational waves from the asymmetric-dark-matter generating phase transition*," JCAP **1705** (2017) no. 05, 028, arXiv:1702.02117.

[11] D. Croon, V. Sanz, and G. White, "*Model Discrimination in Gravitational Wave spectra from Dark Phase Transitions*," arXiv:1806.02332.

[12] M. Cirelli, N. Fornengo, and A. Strumia, "*Minimal dark matter*," Nucl. Phys. **B 753** (2006) 178–194, arXiv:hep-ph/0512090.

[13] T. Hambye, "*Hidden vector dark matter*," JHEP **01** (2009) 028, arXiv:0811.0172.

[14] O. Lebedev, H. M. Lee, and Y. Mambrini, "*Vector Higgs-portal dark matter and the invisible Higgs*," Phys. Lett. **B 707** (2012) 570–576, arXiv:1111.4482.

[15] O. Cata and A. Ibarra, "*Dark Matter Stability without New Symmetries*," Phys. Rev. **D 90** (2014) no. 6, 063509, arXiv:1404.0432.

[16] G. Arcadi, C. Gross, O. Lebedev, Y. Mambrini, S. Pokorski, and T. Toma, "*Multicomponent Dark Matter from Gauge Symmetry*," JHEP **12** (2016) 081, arXiv:1611.00365.

[17] Y. Hochberg, E. Kuflik, H. Murayama, T. Volansky, and J. G. Wacker, "*Model for Thermal Relic Dark Matter of Strongly Interacting Massive Particles*," Phys. Rev. Lett. **115** (2015) no. 2, 021301, arXiv:1411.3727.

[18] T. Hambye and A. Strumia, "*Dynamical generation of the weak and Dark Matter scale*," Phys. Rev. **D 88** (2013) 055022, arXiv:1306.2329.

[19] T. Hambye, A. Strumia, and D. Teresi, "*Super-cool Dark Matter*," JHEP **08** (2018) 188, arXiv:1805.01473.

[20] E. Thrane and J. D. Romano, "*Sensitivity curves for searches for gravitational-wave backgrounds*," Phys. Rev. **D 88** (2013) no. 12, 124032, arXiv:1310.5300.

[21] S. R. Coleman and E. J. Weinberg, "*Radiative Corrections as the Origin of Spontaneous Symmetry Breaking*," Phys. Rev. **D 7** (1973) 1888–1910.

[22] E. Gildener and S. Weinberg, "*Symmetry Breaking and Scalar Bosons*," Phys. Rev. **D 13** (1976) 3333.

[23] N. Bernal, X. Chu, C. Garcia-Cely, T. Hambye, and B. Zaldivar, "*Production Regimes for Self-Interacting Dark Matter*," JCAP **1603** (2016) no. 03, 018, arXiv:1510.08063.

[24] **XENON**, E. Aprile *et al.*, "*First Dark Matter Search Results from the XENON1T Experiment*," Phys. Rev. Lett. **119** (2017) no. 18, 181301, arXiv:1705.06655.

[25] **PandaX-II**, X. Cui *et al.*, "*Dark Matter Results From 54-Ton-Day Exposure of PandaX-II Experiment*," Phys. Rev. Lett. **119** (2017) no. 18, 181302, arXiv:1708.06917.

[26] **LUX**, D. S. Akerib *et al.*, "*Results from a search for dark matter in the complete LUX exposure*," Phys. Rev. Lett. **118** (2017) no. 2, 021303, arXiv:1608.07648.

[27] **XENON**, E. Aprile *et al.*, "*Physics reach of the XENON1T dark matter experiment*," JCAP **1604** (2016) no. 04, 027, arXiv:1512.07501.

[28] **LZ**, D. S. Akerib *et al.*, "*LUX-ZEPLIN (LZ) Conceptual Design Report*," arXiv:1509.02910.

[29] B. J. Mount *et al.*, "*LUX-ZEPLIN (LZ) Technical Design Report*," arXiv:1703.09144.

[30] **DARWIN**, J. Aalbers *et al.*, "*DARWIN: towards the ultimate dark matter detector*," JCAP **1611** (2016) 017, arXiv:1606.07001.

[31] J. M. Moreno, M. Quiros, and M. Seco, "*Bubbles in the supersymmetric standard model*," Nucl. Phys. **B 526** (1998) 489–500, arXiv:hep-ph/9801272.

[32] D. Bodeker and G. D. Moore, "*Can electroweak bubble walls run away?*," JCAP **0905** (2009) 009, arXiv:0903.4099.

[33] D. Bodeker and G. D. Moore, "*Electroweak Bubble Wall Speed Limit*," JCAP **1705** (2017) no. 05, 025, arXiv:1703.08215.

[34] M. Hindmarsh, S. J. Huber, K. Rummukainen, and D. J. Weir, "*Gravitational waves from the sound of a first order phase transition*," Phys. Rev. Lett. **112** (2014) 041301, arXiv:1304.2433.

[35] M. Hindmarsh, S. J. Huber, K. Rummukainen, and D. J. Weir, "*Numerical simulations of acoustically generated gravitational waves at a first order phase transition*," Phys. Rev. **D 92** (2015) no. 12, 123009, arXiv:1504.03291.

[36] M. Hindmarsh, S. J. Huber, K. Rummukainen, and D. J. Weir, "*Shape of the acoustic gravitational wave power spectrum from a first order phase transition*," Phys. Rev. **D 96** (2017) no. 10, 103520, arXiv:1704.05871.

[37] C. Caprini, R. Durrer, and G. Servant, "*The stochastic gravitational wave background from turbulence and magnetic fields generated by a first-order phase transition*," JCAP **0912** (2009) 024, arXiv:0909.0622.

[38] P. Binetruy, A. Bohe, C. Caprini, and J.-F. Dufaux, "*Cosmological Backgrounds of Gravitational Waves and eLISA/NGO: Phase Transitions, Cosmic Strings and Other Sources*," JCAP **1206** (2012) 027, arXiv:1201.0983.

[39] A. Kosowsky, M. S. Turner, and R. Watkins, "*Gravitational radiation from colliding vacuum bubbles*," Phys. Rev. **D 45** (1992) 4514–4535.

[40] A. Kosowsky, M. S. Turner, and R. Watkins, "*Gravitational waves from first order cosmological phase transitions*," Phys. Rev. Lett. **69** (1992) 2026–2029.

[41] A. Kosowsky and M. S. Turner, "*Gravitational radiation from colliding vacuum bubbles: envelope approximation to many bubble collisions*," Phys. Rev. **D 47** (1993) 4372–4391, arXiv:astro-ph/9211004.

[42] M. Kamionkowski, A. Kosowsky, and M. S. Turner, "*Gravitational radiation from first order phase transitions*," Phys. Rev. **D 49** (1994) 2837–2851, arXiv:astro-ph/9310044.

[43] C. Caprini, R. Durrer, and G. Servant, "*Gravitational wave generation from bubble collisions in first-order phase transitions: An analytic approach*," Phys. Rev. **D 77** (2008) 124015, arXiv:0711.2593.

[44] S. J. Huber and T. Konstandin, "*Gravitational Wave Production by Collisions: More Bubbles*," JCAP **0809** (2008) 022, arXiv:0806.1828.

[45] J. R. Espinosa, T. Konstandin, J. M. No, and G. Servant, "*Energy Budget of Cosmological First-order Phase Transitions*," JCAP **1006** (2010) 028, arXiv:1004.4187.

[46] A. J. Farmer and E. S. Phinney, "*The gravitational wave background from cosmological compact binaries*," Mon. Not. Roy. Astron. Soc. **346** (2003) 1197, arXiv:astro-ph/0304393.

[47] P. A. Rosado, "*Gravitational wave background from binary systems*," Phys. Rev. **D 84** (2011) 084004, arXiv:1106.5795.

[48] D. I. Kosenko and K. A. Postnov, "*On the gravitational wave noise from unresolved extragalactic binaries*," Astron. Astrophys. **336** (1998) 786, arXiv:astro-ph/9801032.

[49] G. Nelemans, L. R. Yungelson, and S. F. Portegies Zwart, "*The gravitational wave signal from the galactic disk population of binaries containing two compact objects*," Astron. Astrophys. **375** (2001) 890–898, arXiv:astro-ph/0105221.

[50] A. J. Ruiter, K. Belczynski, M. Benacquista, S. L. Larson, and G. Williams, "*The LISA Gravitational Wave Foreground: A Study of Double White Dwarfs*," Astrophys. J. **717** (2010) 1006–1021, arXiv:0705.3272.

[51] M. R. Adams and N. J. Cornish, "*Discriminating between a Stochastic Gravitational Wave Background and Instrument Noise*," Phys. Rev. **D 82** (2010) 022002, arXiv:1002.1291.

[52] M. R. Adams and N. J. Cornish, "*Detecting a Stochastic Gravitational Wave Background in the presence of a Galactic Foreground and Instrument Noise*," Phys. Rev. **D 89** (2014) no. 2, 022001, arXiv:1307.4116.

[53] C. Cutler and J. Harms, "*BBO and the neutron-star-binary subtraction problem*," Phys. Rev. **D 73** (2006) 042001, arXiv:gr-qc/0511092.

[54] **Virgo, LIGO Scientific**, B. P. Abbott *et al.*, "*GW170817: Implications for the Stochastic Gravitational-Wave Background from Compact Binary Coalescences*," Phys. Rev. Lett. **120** (2018) no. 9, 091101, arXiv:1710.05837.

[55] E. Witten, "*Cosmological Consequences of a Light Higgs Boson*," Nucl. Phys. **B 177** (1981) 477–488.

[56] A. H. Guth and E. J. Weinberg, "*A Cosmological Lower Bound on the Higgs Boson Mass*," Phys. Rev. Lett. **45** (1980) 1131.

[57] W. Buchmuller and D. Wyler, "*The Effect of dilatons on the electroweak phase transition*," Phys. Lett. **B 249** (1990) 281–285.

[58] V. A. Kuzmin, M. E. Shaposhnikov, and I. I. Tkachev, "*Strong CP violation, electroweak baryogenesis, and axionic dark matter*," Phys. Rev. **D 45** (1992) 466–475.

[59] J. R. Espinosa, T. Konstandin, J. M. No, and M. Quiros, "*Some Cosmological Implications of Hidden Sectors*," Phys. Rev. **D 78** (2008) 123528, arXiv:0809.3215.

[60] T. Konstandin and G. Servant, "*Cosmological Consequences of Nearly Conformal Dynamics at the TeV scale*," JCAP **1112** (2011) 009, arXiv:1104.4791.

[61] D. Spolyar, "*SuperCool Inflation: A Graceful Exit from Eternal Inflation at LHC Scales and Below*," arXiv:1111.3629.

[62] G. C. Dorsch, S. J. Huber, and J. M. No, "*Cosmological Signatures of a UV-Conformal Standard Model*," Phys. Rev. Lett. **113** (2014) 121801, arXiv:1403.5583.

[63] J. Jaeckel, V. V. Khoze, and M. Spannowsky, "*Hearing the signal of dark sectors with gravitational wave detectors*," Phys. Rev. **D 94** (2016) no. 10, 103519, arXiv:1602.03901.

[64] R. Jinno and M. Takimoto, "*Probing a classically conformal B-L model with gravitational waves*," Phys. Rev. **D 95** (2017) no. 1, 015020, arXiv:1604.05035.

[65] J. Kubo and M. Yamada, "*Scale genesis and gravitational wave in a classically scale invariant extension of the standard model*," JCAP **1612** (2016) no. 12, 001, arXiv:1610.02241.

[66] A. Kobakhidze, C. Lagger, A. Manning, and J. Yue, "*Gravitational waves from a supercooled electroweak phase transition and their detection with pulsar timing arrays*," Eur. Phys. J. **C 77** (2017) no. 8, 570, arXiv:1703.06552.

[67] K. Tsumura, M. Yamada, and Y. Yamaguchi, "*Gravitational wave from dark sector with dark pion*," JCAP **1707** (2017) no. 07, 044, arXiv:1704.00219.

[68] L. Marzola, A. Racioppi, and V. Vaskonen, "*Phase transition and gravitational wave phenomenology of scalar conformal extensions of the Standard Model*," Eur. Phys. J. **C 77** (2017) no. 7, 484, arXiv:1704.01034.

[69] S. Iso, P. D. Serpico, and K. Shimada, "*QCD-Electroweak First-Order Phase Transition in a Supercooled Universe*," Phys. Rev. Lett. **119** (2017) no. 14, 141301, arXiv:1704.04955.

[70] M. Aoki, H. Goto, and J. Kubo, "*Gravitational Waves from Hidden QCD Phase Transition*," Phys. Rev. **D 96** (2017) no. 7, 075045, arXiv:1709.07572.

[71] S. Arunasalam, A. Kobakhidze, C. Lagger, S. Liang, and A. Zhou, "*Low temperature electroweak phase transition in the Standard Model with hidden scale invariance*," Phys. Lett. **B 776** (2018) 48–53, arXiv:1709.10322.

[72] B. von Harling and G. Servant, "*QCD-induced Electroweak Phase Transition*," JHEP **01** (2018) 159, arXiv:1711.11554.

[73] D. Huang and B.-Q. Lu, "*Comment on "Hearing the signal of dark sectors with gravitational wave detectors"*," Phys. Rev. **D 97** (2018) no. 6, 068303, arXiv:1803.03180.

[74] K. Griest and M. Kamionkowski, "*Unitarity Limits on the Mass and Radius of Dark Matter Particles*," Phys. Rev. Lett. **64** (1990) 615.

[75] I. Baldes and K. Petraki, "*Asymmetric thermal-relic dark matter: Sommerfeld-enhanced freeze-out, annihilation signals and unitarity bounds*," JCAP **1709** (2017) no. 09, 028, arXiv:1703.00478.

[76] H. L. Child and J. T. Giblin, Jr., "*Gravitational Radiation from First-Order Phase Transitions*," JCAP **1210** (2012) 001, arXiv:1207.6408.

[77] T. Regimbau, "*The astrophysical gravitational wave stochastic background*," Res. Astron. Astrophys. **11** (2011) 369–390, arXiv:1101.2762.

[78] R. D. Pisarski and F. Wilczek, "*Remarks on the Chiral Phase Transition in Chromodynamics*," Phys. Rev. **D 29** (1984) 338–341.

[79] F. R. Brown, F. P. Butler, H. Chen, N. H. Christ, Z.-h. Dong, W. Schaffer, L. I. Unger, and A. Vaccarino, "*On the existence of a phase transition for QCD with three light quarks*," Phys. Rev. Lett. **65** (1990) 2491–2494.

[80] J. Elias-Miro, J. R. Espinosa, and T. Konstandin, "*Taming Infrared Divergences in the Effective Potential*," JHEP **08** (2014) 034, arXiv:1406.2652.

[81] M. E. Carrington, "*The Effective potential at finite temperature in the Standard Model*," Phys. Rev. **D 45** (1992) 2933–2944.